Supporting Information

Highly graphitic carbon nanosheets synthesized over the tailored mesoporous molecular sieves using acetylene by chemical vapor deposition method

Raji Atchudan,*[a] Suguna Perumal[b], Thomas Nesakumar Jebakumar Immanuel Edison[a] and Yong Rok Lee*[a]

[a]*School of Chemical Engineering, Yeungnam University, Gyeongsan 712-749, Republic of Korea*

[b]*Department of Applied Chemistry, Kyungpook National University, Daegu 702-701, Republic of Korea*

*Corresponding authors: E-mail: atchudanr@yu.ac.kr (R. Atchudan); yrlee@yu.ac.kr (Y. R. Lee)

Table S1: Textural properties of mesoporous Si-MCM-41 and Ti-MCM-41 molecular sieves.

S. No	**Catalytic template (Si/Ti ratio)[a]**	**(Si/Ti ratio)[b]**	**d-spacing value (Å)[c]**	**Surface area (m^2/g)[d]**	**Pore size (Å)[d]**	**Pore volume (cm^3/g)[d]**
1	Si-MCM-41	--	36.5	1150	29.5	0.90
2	Ti-MCM-41 (100)	102	36.2	1100	29.0	0.88
3	Ti-MCM-41 (75)	77	36.0	1070	28.7	0.87
4	Ti-MCM-41 (50)	53	35.7	980	28.3	0.84
5	Ti-MCM-41 (25)	29	35.5	870	27.7	0.80

[a]The values are calculated from the gel

[b]The values obtained from ICP-AES analysis

[c]The values calculated from XRD analysis

[d]The values obtained from N_2 physisorption studies

XRD analysis of mesoporous Si-MCM-41 and Ti-MCM-41 molecular sieves

The small-angle XRD patterns of as-synthesised and calcined mesoporous Si-MCM-41 and Ti-MCM-41 molecular sieves with various Si/Ti ratios are shown in Fig. S1. XRD pattern show that samples exhibit an intense diffraction peak in the range of 2.0–2.3° (2θ) due to (100) diffraction plane and low intense peaks in the range of 4.0–6.5° (2θ) due to (110), (200), and (210) diffraction planes confirming the formation of well-ordered mesoporous MCM-41 molecular sieves with hexagonal regularity. The calcined materials possess well-defined pore structure due to the condensation of Si–OH groups. The XRD patterns of the calcined mesoporous Si-MCM-41 molecular sieves are same as as-synthesized mesoporous Si-MCM-41 molecular sieves which confirmed the absence of structural damage of Si-MCM-41 during the calcination. After calcination of mesoporous Si-MCM-41 molecular sieves, the d-spacing value is shifted towards the higher values and 2θ value is shifted to lower region, implying expand in the unit cell as a result of the removal of the surfactant molecules used as structure directing agent. The occluded surfactant molecules escape from the host mesoporous Si-MCM-41 molecular sieves during the calcination. After removal of surfactant, the pore will be clear thus the interlayer distance shifts towards higher values. The XRD patterns obtained are found to be in good agreement with a previous report for similar mesoporous MCM-41 molecular sieves.[S1,S2] The 2θ value of Ti-MCM-41 is little higher than Si-MCM-41 because pore shrinkage occurred during the incorporation of Ti metal particles over the mesoporous MCM-41 molecular sieves. The 2θ value is smaller and extents gradually to higher region for metal incorporated MCM-41 molecular sieves from Ti-MCM-41 (100) to Ti-MCM-41 (25) which is clear from XRD pattern. The d-spacing value decreases with increase in Ti concentration over the mesoporous MCM-41 molecular sieve implying shrinkage in the unit cell as a result of the addition (incorporation) of

the Ti metal nanoparticle over the mesoporous support. While increasing the Ti concentration, though the intensity of the peak decreases, but the pattern remains unchanged. Insets of the magnified view of XRD patterns of mesoporous Si-MCM-41 and Ti-MCM-41 molecular sieves with various Si/Ti ratios are shown. All the patterns of mesoporous MCM-41 molecular sieves are clearly seen and only the intensity gradually decreases with increase in the metal concentration over the mesoporous support but the crystallinity is not much affected which is clearer from inset image. This observation strongly suggest, there is no the structural damage in the mesoporous MCM-41 molecular sieves after incorporation of Ti in large amounts. The d-spacing value (d) is calculated using Bragg equation (S1) based on the position of (100) reflection peak.

$$n\lambda = 2d\sin\theta \quad \text{(or)} \qquad d = \frac{n\lambda}{2\sin\theta} \qquad \text{(S1)}$$

where, n is an integer (1), λ is the wavelength of incident wave (1.54 Å), and θ is the angle between the incident ray and the scattering planes. The d-spacing values of synthesized mesoporous Si-MCM-41 and Ti-MCM-41 molecular sieves with various Si/Ti ratios are shown in Table S1. Apart from that, the study strongly suggests the synthesized mesoporous MCM-41 molecular sieve having high structural ordering.

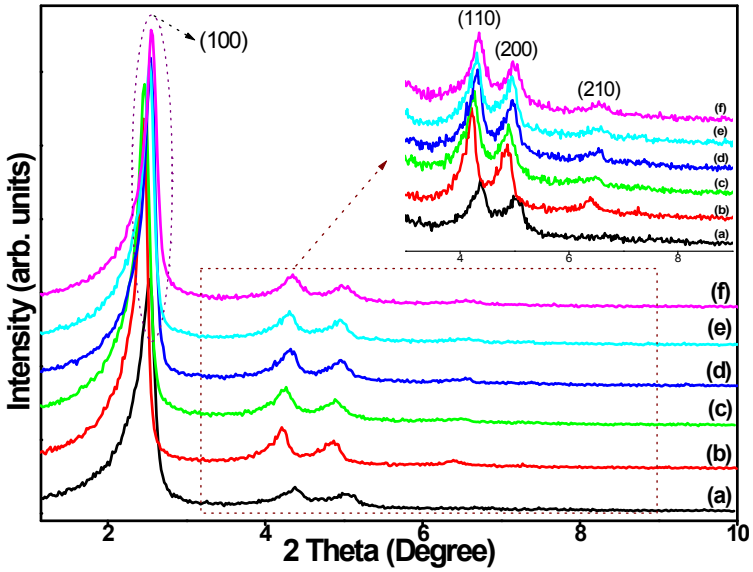

Fig. S1 XRD patterns of as-synthesised (a) Si-MCM-41, calcined (b)Si-MCM-41, (c) Ti-MCM-41 (100), (d) Ti-MCM-41 (75), (e) Ti-MCM-41 (50) and (f) Ti-MCM-41 (25).

FT-IR spectroscopy analysis of mesoporous Si-MCM-41 and Ti-MCM-41 molecular sieves

FT-IR spectroscopy technique has been used extensively for the identification of functional group of nanomaterials. The FT-IR spectra of the as-synthesized mesoporous Si-MCM-41 and Ti-MCM-41 molecular sieves with various Si/Ti ratios are shown in Fig. S2A. The broad band around 3450 cm^{-1} may be attributed to surface silanol groups and physically adsorbed water molecules, while deformational vibrations of adsorbed molecules caused the absorption bands at 1645 cm^{-1}.[S3] In the FT-IR spectra of as-synthesized Si-MCM-41 and Ti-MCM-41, the absorption bands around 2925 and 2857 cm^{-1} corresponds to asymmetric and symmetric stretching vibrations of the surfactant molecules (structure directing agent). The corresponding bending mode is observed at 1487 and 1460 cm^{-1}. The peaks between 450 and 1250 cm^{-1} are assigned to framework vibrations of mesoporous silica. The asymmetric and symmetric stretching vibration bands of framework Si-O-Si bands appeared at 1065 and 800 cm^{-1} are assigned for porous silica material.[S4] The band at 467 cm^{-1} is assigned to bending mode of Si-O-Si bonds in their respective catalysts. Additionally, absorption band at 967 cm^{-1} is also assigned to a stretching vibration of Si-O-Si/Si-O-Ti/Ti-Si-Ti linkages by metal incorporation of silanol.[S5] The band at 2365 cm^{-1} corresponds to the asymmetric stretching vibration of CO_2 originating from ambient air absorbed in the optical path outside the FT-IR cell and also CO_2 molecules adsorbed over the mesoporous frame work. Fig. 2SB shows the FT-IR spectra of the calcined mesoporous Si/MCM-41 and Ti-MCM-41 molecular sieves with various Si/Ti ratios. The characteristic asymmetric and symmetric stretching vibrations bands for $–CH_2$ of structure directing agent observed in as-synthesized mesoporous MCM-41 molecular sieves at 2857 and 2925 cm^{-1} disappear in the calcined samples. Also, the corresponding bending mode at 1487 and 1460 cm^{-1} also disappear in the calcined samples. This strongly reveals that the structure directing agent is

completely removed from the host mesoporous MCM-41 molecular sieves after calcination. All the other bands seem to be unaffected, which implies that there is no structural deformation even after calcination. This result strongly suggests that synthesized mesoporous materials are having high structural stability and thermal stability which is further confirmed by thermogravimetric analysis.

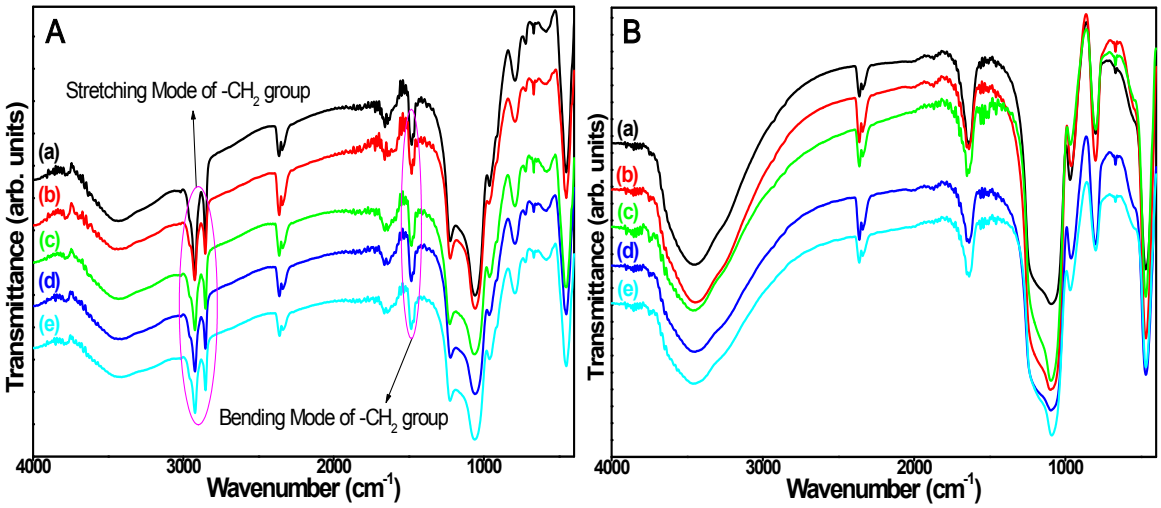

Fig. S2 FT-IR spectra of (A) as-synthesised and (B) calcined (a) Si-MCM-41, (b) Ti-MCM-41 (100), (c) Ti-MCM-41 (75), (d) Ti-MCM-41 (50), (e) Ti-MCM-41 (25).

Thermogravimetric analysis of mesoporous Si-MCM-41 and Ti-MCM-41 molecular sieves

The thermal stability is one the important factors to decide the catalytic activity of mesoporous materials for the production of graphitic carbon nanostructures at the moderate reaction temperature. The TG/DTA of the as-synthesised mesoporous Si-MCM-41 and Ti-MCM-41 molecular sieves with various Si/Ti ratios is shown in Fig. S3. The thermograms show three distinguish weight losses; there is an initial weight loss below 150 °C due to desorption/ decomposition of physically adsorbed water molecules over the host mesoporous Si-MCM-41 and Ti-MCM-41 molecular sieves. The second major weight loss due to decomposition and desorption of occluded organic template (structure directing agent) occurs between 150 and 350 °C. This is followed by final minute quantity of weight loss between 350 and 550 °C which is ascribed to water loss from the condensation of adjacent silanol (Si-OH) groups to form siloxane (Si-O-) bond.[S6,S7] Further, we observe the absence of decomposition up to 1000 °C from the thermogram which is credited to thermal stability of the material, and structural ordering of the mesoporous mesoporous MCM-41 molecular sieves material after calcination. The wt% of residue slightly increases with increase in the Ti content over the mesoporous host material. The weight loss majorly depends on the amount of surfactant, as more the number of surfactant molecules occluded in the host mesoporous Si-MCM-41 molecular sieves the more is the weight loss. The percentage of occupied surfactant molecules in the host material depends on the pore size and pore volume of the mesoporous material. The Ti-MCM-41 with Si/Ti ratio 25 was high residual percentage compared to other Si/Ti ratios and also Si-MCM-41. This might be due to shrinkage of pore size and volume while increasing the Ti content over the mesoporous MCM-41 molecular sieve. The three distinguished weight losses are very clear from DTA curves and are marked as circles in inset Fig. S3.

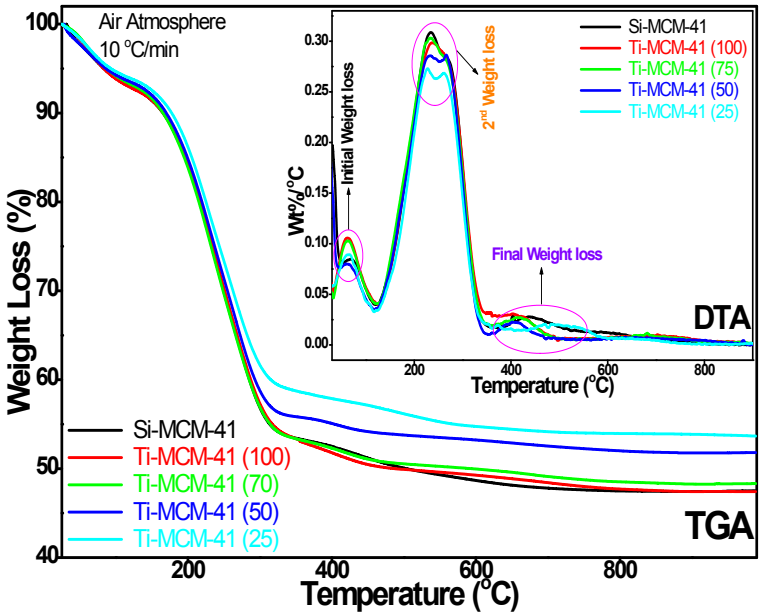

Fig. S3 TG/DTA curves of as-synthesized Si-MCM-41 and Ti-MCM-41

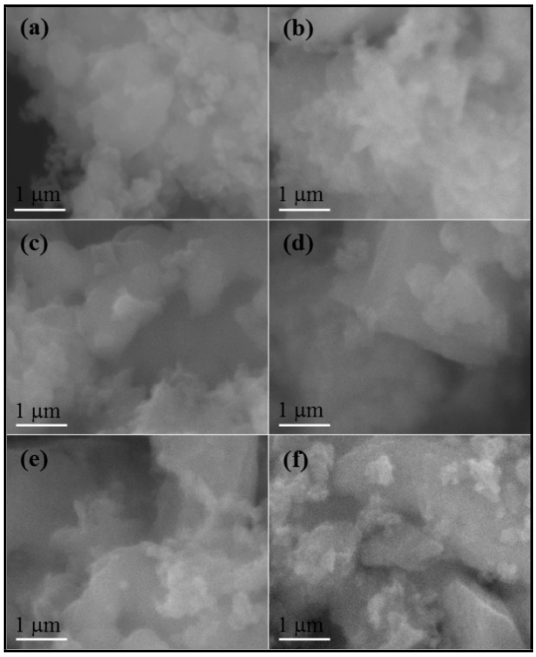

Fig. S4 SEM images of calcined (a) Si-MCM-41, (b) Ti-MCM-41 (100), (c) Ti-MCM-41 (75), (d) Ti-MCM-41 (50), (e) Ti-MCM-41 (25) and (f) Ti-MCM-41 (20).

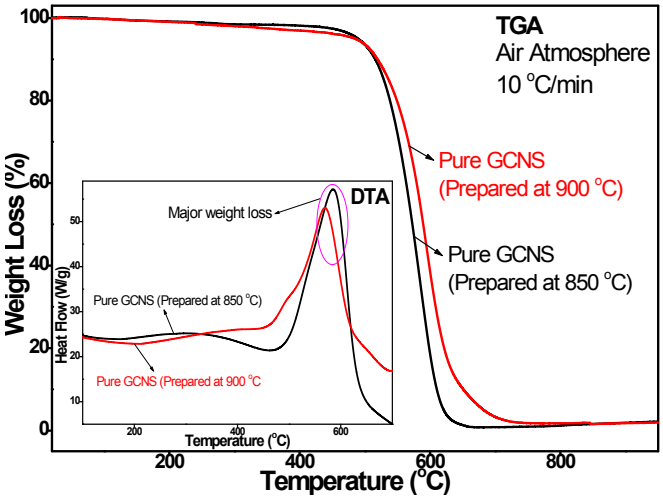

Fig. S5 TG/DTA curves of GCNS resulted from Ti-MCM-41 (75) at (a) 850 and (b) 900 ºC.

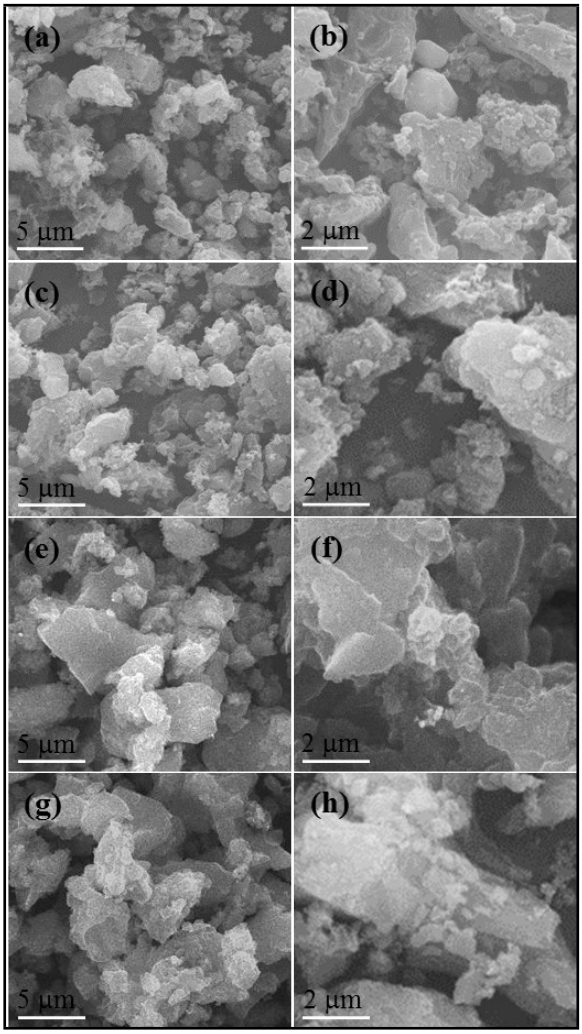

Fig. S6 SEM images of GCNS with different magnifications obtained over the Ti-MCM-41 with various Si/Ti ratios (a and b) 25, (c and d) 50, (e and f) 75 and (g and h) 100 at 850 °C.

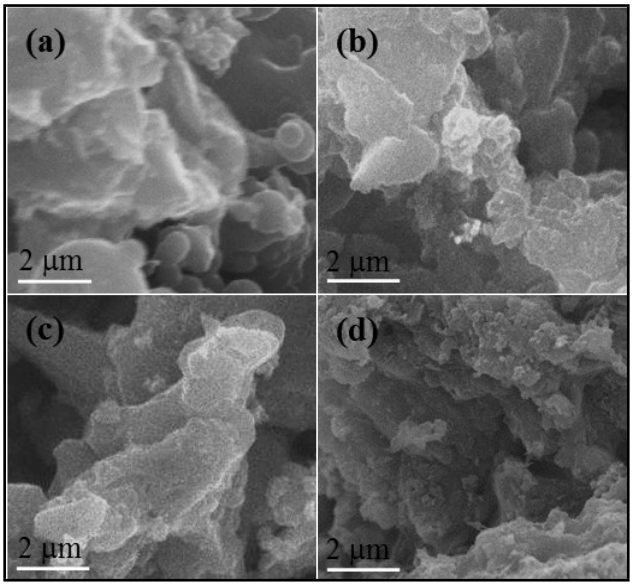

Fig. S7 SEM images of GCNS obtained over the Ti-MCM-41 (75) at (a) 800, (b) 850, (c) 900 and (d) 950 °C.

HRTEM analysis of GCNS

The HRTEM images of GCNS resulting from mesoporous Ti-MCM-41 molecular sieves with various Si/Ti ratios at the reaction temperature of 850 °C are shown in Fig. S8. The formed GCNS are graphitic in nature and graphene sheet damage increases with increase in metal content over the mesoporous MCM-41 molecular sieves. The mesoporous Ti-MCM-41 molecular sieves produced GCNS without any major defects and results in larger GCNS. The HR-TEM images of GCNS obtained over the Ti-MCM-41 do not have much variation by varying concentration of Ti concentration. The graphitization of GCNS increases with increase in Ti content over the mesoporous MCM-41 molecular sieves; beyond the optimum level the degree of graphitization decreased which is confirmed by Raman spectrum and XRD results. This might be due to the fact that carbon nanosheets are grown on the Ti nanoparticles over the mesoporous MCM-41 molecular sieves, while increasing the Ti concentration over the mesoporous MCM-41 molecular sieves for the formation of GCNS which results in increase in the carbon nanosheets. The above said statement was concluded by TGA calculation yield of GCNS depends of Ti concentration. After removing the catalytic template with Ti nanoparticles, it makes hole/split carbon nanosheets. Thus, the result suggests that the metal content is playing important role for the growth of GCNS with well graphitization.

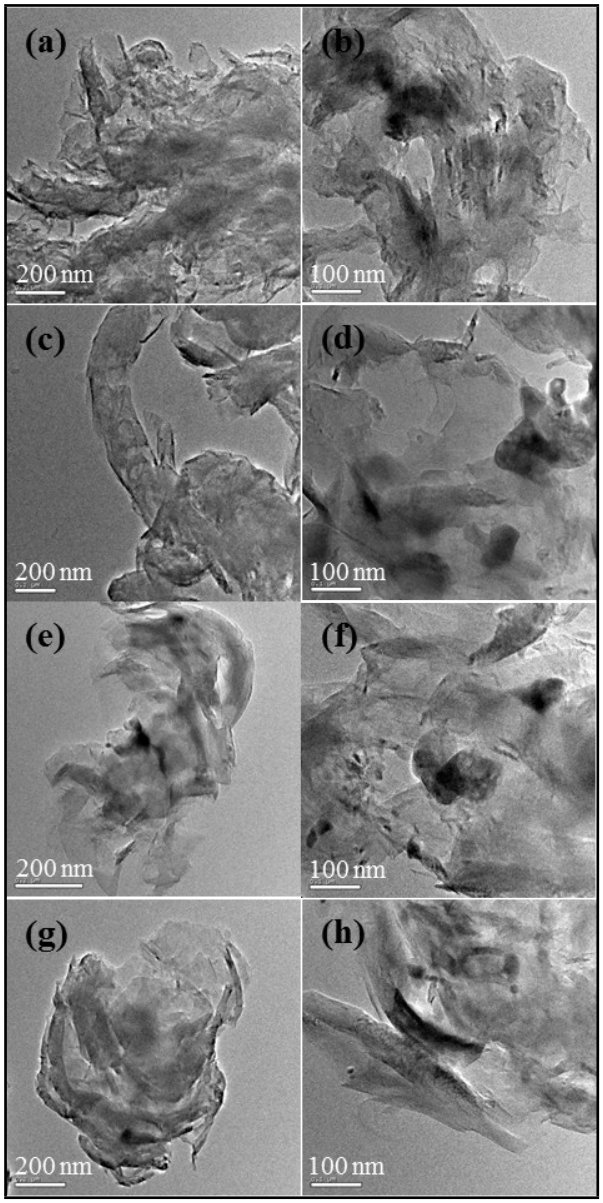

Fig. S8 TEM images of GCNS obtained over the Ti-MCM-41 with various Si/Ti ratios (a and b) 25, (c and d) 50, (e and f) 75 and (g and h) 100 at 850 °C.

References

S1 J. Sui, C. Zhang, D. Hong, J. Li, Q. Cheng, Z. Lib and W. Cai, *J. Mater. Chem*., 2012, **22**, 13674–13681.

S2 J. C. Juan, Y. Jiang, X. Meng, W. Cao, M. A. Yarmo and J. C. Zhang, *Mater. Res. Bull*., 2007, **42**, 1278–1285.

S3 A. V. Kiseler and V. I. Lygin, Infrared Spectra of Surface Compounds and Adsorbed Substances, Nauka, Moscow, Russian, 1992.

S4 V. Umamaheswari, M. Palanichamy and V. Murugesan, *J. Catal*., 2002, **210**, 367–374.

S5 K. A. Koyano and T. Tatsumi, *Chem. Commun*., 1996, 145–146.

S6 M. L. Occelli, S. Biz, A. Auroux and G. J. Ray, *Micropor. Mesopor. Mater*., 1998, **26**, 193–213.

S7 C. Y. Chen, H. X. Li and M. E. Davis, *Micropor. Mater*. 1993, **2**, 17–26.